Supporting Information

Thionaphthalimide-based photosensitizer for efficient photodynamic therapy

Qian Chen[a,1], Lingyu Jin[b,c,1], Jia Hong[a,1], Ming-Ming Sun[a], Xuefei Huang[b,c], Yangjie Liu[b,c], Wen Xiu Ren[b,c*], Qian-Yong Cao[a,*],

[a]*College of Chemistry and Chemical Engineering, Nanchang University, Nanchang 330031, P. R. China*
[b]*Department of Radiology, the Affiliated Hospital of Southwest Medical University, Luzhou 646000, China*
[c]*Precision Imaging and Intelligent Analysis Key Laboratory of Luzhou City, Luzhou 646000, China.*

E-mail: cqyong@ncu.edu.cn (Q.-Y. Cao), xrenwenxiux@swmu.edu.cn (W.X. Ren)

Experimental section

Materials and equipment

9,10-Anthracenediyl-bis(methylene)dimalonic acid (ABDA), tetraethylethylene glycol monomethyl ester, 4-bromo-1,8-naphthalenedicarboxylic anhydride, 4-bromotriphenylamine, *p*-aminophenol, 2′,7′-dichlorodihydrofluorescein diacetate (DCFH-DA) and dihydroethidium (DHE) were purchased from Shanghai Macklin Reagent Co., Ltd. Tetrakis(triphenylphosphine)palladium and Lawson's reagent were purchased from Tansoole Reagent Company. Propidium iodide (PI) and calcein were purchased from Beyotime Biotechnology Co., Ltd. All chemicals and solvents were of analytical grade and used without further purification. 4-(Diphenylamino)benzeneboronic acid pinacol ester and tetraethyleneglycol mono-p-toluenesulfonate were prepared according to the reported literature.

Emission and absorption spectra were measured by Hitach F-4500 fluorescence spectrophotometer and Hitachi UV-3010 spectrophotometer. The ^{1}H NMR and ^{13}C NMR spectra were measured by using a Varian instrument (400 MHz). Size distribution and zeta potential were used by Zetasizer Nano-ZS90. Zeiss LSM 710 laser scanning confocal microscopy was used for cell imaging. Agilent LC/MSD TRAP XCT Plus was used to record HRMS spectra.

Synthesis

Synthesis of NI-Br: A mixture of 4-bromo-1,8- naphthalic anhydride (2.0 g, 7.2 mmol), 4-hydroxyaniline (1.6 g, 14.4 mmol) and 20 mL of glacial acetic acid was refluxed for overnight. After the reaction was completed and cooled to room temperature, the solution was poured into ice water. The gray solid product was obtained by suction filtration, and washed with a large amount of water. The crude product was purified by silica gel column chromatography using dichloromethane/petroleum ether (v/v = 4:1) as eluent. The product NI-Br was obtained as an off-white powder in 65% yield. ^{1}H NMR (400 MHz, $CDCl_3$) δ (ppm): 8.70 (d, *J* = 7.2 Hz, 1H), 8.64 (d, *J* = 8.5 Hz, 1H), 8.46 (d, *J* = 7.9 Hz, 1H), 8.08 (d, *J* = 7.9 Hz, 1H), 7.89 (dd, *J* = 8.5, 7.4 Hz, 1H), 7.16 (d, *J* = 8.4 Hz, 2H), 6.96 (d, *J* = 8.2 Hz, 2H). ^{13}C NMR (101 MHz, DMSO) δ (ppm): 163.81, 163.75, 149.06, 132.88, 131.94, 131.70, 131.30, 130.18, 129.55, 129.40, 129.14, 128.92, 123.90, 123.76, 122.98, 114.17, 40.58, 40.38, 40.17, 39.96, 39.75, 39.54, 39.33. TOF-HRMS (m/z): Calcd. for ($C_{18}H_{10}BrNO_3$): 405.9476 ($M + K^+$), found 405.9473.

Synthesis of TNI: NI-Br (1.12 g, 2.10 mmol), 4-(diphenylaminophenyl) boronic acid pinacol ester (1.02 g, 2.73 mmol), K_2CO_3 (1.16 g, 8.4 mmol), and $Pd(PP_3)_4$（0.026 g, 0.18 mmol） were dissolved in 30 ml of anhydrous THF and reacted at reflux overnight. After the reaction was completed, ice water was added to burst the reaction. Subsequently, the product was extracted three times with dichloromethane, and after evaporating the solvent under reduced pressure, the crude product was purified by silica gel column chromatography using dichloromethane/petroleum ether (v/v = 6:1) as the eluent. The product **TNI** was obtained as a pale-yellow powder with a yield of 81%.^{1}H NMR (400 MHz, $CDCl_3$) δ (ppm): 8.69 (d, *J* = 1.6 Hz, 1H), 8.68 – 8.66 (m, 1H), 8.47 (dd, *J* = 8.5, 1.2 Hz, 1H), 7.76 (dd, *J* = 8.9, 7.3 Hz, 2H), 7.42 – 7.37 (m, 2H), 7.33 (dd, *J* = 8.5, 7.2 Hz, 4H), 7.24 – 7.19 (m, 6H), 7.18 – 7.07 (m, 5H), 6.93 – 6.89 (m, 2H). ^{13}C NMR (101 MHz, $CDCl_3$) δ (ppm): 164.99, 164.79, 156.12, 148.44, 147.30, 147.26, 133.31, 131.78, 131.73, 131.49, 130.81, 130.16, 129.52, 129.48, 129.34, 129.23, 127.78, 127.56,

126.77, 125.07, 123.66, 123.53, 122.94, 122.46, 121.25, 116.58, 77.31, 77.00, 76.68. TOF-HRMS (m/z): Calcd. for ($C_{36}H_{24}N_2O_3$): 533.1860 ($M + H^+$), found 533.1851.

Synthesis of TNI-TEG: TNI (0.6 g, 1.12 mmol), tetraethyleneglycol mono-*p*-toluenesulfonate (0.6 g, 1.68 mmol), and K_2CO_3 (0.77 g, 5.60 mmol) were dissolved in 15 ml anhydrous acetone and reacted at reflux for 24 h. After the reaction was completed, ice water was added to burst the reaction. Subsequently, the product was extracted three times with dichloromethane, and after evaporating the solvent under reduced pressure, the crude product was purified by silica gel column chromatography, using dichloromethane/petroleum ether (v/v = 8:1) as eluent. The product **TNI-PEG** was obtained as a bright yellow powder in 73% yield. ^{1}H NMR (400 MHz, $CDCl_3$) δ (ppm): 8.68 – 8.63 (m, 2H), 8.45 (dd, *J* = 8.3, 1.2 Hz, 1H), 7.81 – 7.71 (m, 3H), 7.42 – 7.36 (m, 2H), 7.35 – 7.29 (m, 4H), 7.24 – 7.18 (m, 7H), 7.12 – 7.04 (m, 4H), 4.20 (t, *J* = 4.9 Hz, 2H), 3.92 – 3.86 (m, 2H), 3.72 – 3.59 (m, 12H), 3.38 – 3.36 (m, 3H). ^{13}C NMR (101 MHz, $CDCl_3$) δ (ppm): 164.71, 164.50, 158.76, 148.40, 147.31, 147.06, 133.12, 131.85, 131.54, 131.29, 130.80, 130.16, 129.80, 129.56, 129.48, 129.22, 128.12, 127.97, 127.73, 126.72, 125.05, 123.65, 123.05, 122.47, 121.37, 115.37, 77.35, 77.03, 76.72, 71.94, 71.91, 70.86, 70.73, 70.65, 70.61, 70.59, 70.57, 70.52, 70.50, 69.65, 69.22, 68.67, 67.67, 59.03. TOF-HRMS (m/z): Calcd. for ($C_{45}H_{42}N_2O_7$): 723.3065 ($M + H^+$), found 723.3050.

Synthesis of TNI-OMe: TNI (0.3 g, 0.56 mmol), methyl iodide (0.16 g, 1.12 mmol) and K_2CO_3 (0.39 g, 2.80 mmol) were dissolved in 15 ml of anhydrous acetonitrile and reacted under reflux for 24 h. After the reaction was complete, ice water was added to quench the reaction and the mixture was extracted three times with dichloromethane. After evaporating the solvent under reduced pressure, the crude product was purified by silica gel column chromatography using dichloromethane/petroleum ether (v/v=1:3) as an eluent. The product **TNI-OME** was obtained as a bright yellow powder in 84% yield. ^{1}H NMR (400 MHz, $CDCl_3$) δ (ppm): δ 8.70 – 8.63 (m, 2H), 8.46 (dd, J = 8.4, 1.2 Hz, 1H), 7.75 (dd, J = 8.7, 7.3 Hz, 2H), 7.39 (d, J = 8.3 Hz, 2H), 7.36 – 7.29 (m, 4H), 7.27 – 7.19 (m, 8H), 7.13 – 7.04 (m, 4H), 3.88 (s, 3H). ^{13}C NMR (101 MHz, $CDCl_3$) δ (ppm): 164.75, 164.53, 159.53,

148.41, 147.32, 147.07, 133.12, 131.86, 131.55, 131.30, 130.80, 130.17, 129.56, 129.48, 129.23, 127.97, 127.73, 126.72, 125.05, 123.65, 123.06, 122.48, 121.39, 114.74, 77.33, 77.01, 76.69, 55.49.

Synthesis of TNIS-TEG: TNI-PEG (0.3 g, 0.42 mmol) and Lawson's reagent (0.85 g, 2.13 mmol) were dissolved in 20 ml of anhydrous toluene and reacted at reflux for 36 h. After the reaction was completed, the solvent was spun dry under reduced pressure and the crude product was purified by silica gel column chromatography using dichloromethane/petroleum ether (v/v = 5:1) as the eluent. The product **TNIS-PEG** was obtained as a dark purple powder with a yield of 28%. ^{1}H NMR (400 MHz,$CDCl_3$) δ (ppm): 8.95 (t, *J* = 7.2 Hz, 2H), 8.44 (dd, *J* = 8.4, 1.0 Hz, 1H), 7.63 (dt, *J* = 8.0, 4.0 Hz, 3H), 7.38 (d, *J* = 8.5 Hz, 2H), 7.32 (t, *J* = 7.8 Hz, 5H), 7.22 – 7.17 (m, 6H), 7.13 – 7.05 (m, 7H), 4.20 (t, *J* = 4.9 Hz, 2H), 3.89 (t, *J* = 4.9 Hz, 2H), 3.75 (dd, *J* = 6.2, 3.5 Hz, 3H), 3.72 – 3.61 (m, 10H), 3.38 (d, *J* = 0.6 Hz, 3H). ^{13}C NMR (101 MHz, $CDCl_3$) δ (ppm): 192.68, 192.23, 158.29, 148.52, 147.23, 146.58, 139.22, 137.87, 137.52, 132.78, 131.79, 130.71, 130.05, 130.01, 129.80, 129.50, 129.22, 128.59, 128.42, 127.98, 127.17, 125.13, 124.69, 124.35, 123.75, 122.34, 115.32, 77.34, 77.02, 76.70, 71.95, 71.92, 70.86, 70.73, 70.66, 70.63, 70.58, 70.52, 70.50, 69.66, 69.22, 68.67, 67.46, 59.05. TOF-HRMS (m/z): Calcd. for ($C_{45}H_{42}N_2O_5S_2$): 777.2427 ($M + Na^+$), found 777.2732.

Synthesis of TNIS-OME: Specific synthetic steps refer to the compound **TNIS-PEG**. The product **TNIS-OME** was obtained as a purple-black solid with a yield of 28%. ^{1}H NMR (400 MHz, $CDCl_3$) δ (ppm): 8.99 – 8.91 (m, 2H), 8.43 (dd, J = 8.5, 1.3 Hz, 1H), 7.63 (dt, J = 8.1, 4.1 Hz, 2H), 7.38 (d, J = 8.2 Hz, 2H), 7.36 – 7.29 (m, 4H), 7.25 (s, 1H), 7.23 – 7.19 (m, 5H), 7.13 – 7.04 (m, 6H), 3.88 (s, 3H). ^{13}C NMR (101 MHz, $CDCl_3$) δ (ppm): 192.74, 192.28, 159.06, 148.53, 147.23, 146.61, 139.12, 137.90, 137.55, 132.80, 131.79, 130.71, 130.02, 129.50, 129.22, 128.60, 128.42, 127.18, 125.13, 123.75, 122.34, 114.76, 77.32, 77.00, 76.68, 55.33.

Theoretical calculation and characterization of compounds

All theoretical calculations were performed on the B3LYP/6-31G(d) basis set using the Gaussian 09 program. The optimal geometric configuration of the compound was

calculated by density functional theory in the SMD solvent model H2O medium. In the same medium, the energy level energies of different singlet and triplet states of the compound were calculated by time-dependent density functional theory.

ROS Detection

Total ROS detection by DCFH

Total ROS production capacity of photosensitizers in aqueous solution was detected using 2,7-dichlorodihydrofluorescein (DCFH) as a ROS indicator. DCFH was prepared by pre-hydrolysis of DCFH-DA according to previous reports. Expose a mixture of indicator DCFH (10 μM) and PSs TNPS or MB (10 μM) to white light and record the PL intensity at approximately 525 nm every 10 seconds in a PL spectrofluorometer (excitation wavelength: 490 nm).The fluorescence intensity at 525 nm was recorded to indicate the overall rate of ROS production.

Detection of $^1O_2$ generation by ABDA

Using the commonly used singlet oxygen ($^1O_2$) indicator ABDA to detect the PS under the illumination of white light $^1O_2$ generation ability in aqueous solution, and rose bengal (RB) as the standard singlet oxygen photosensitizer. Expose a mixture of indicator ABDA (60 μM) and **TNPS** or RB (10 μM) to white light and record the absorbance at 383 nm every 10 seconds in a UV spectrophotometer. Record the UV absorbance intensity at 383 nm to indicate the rate of singlet oxygen ($^1O_2$) generation.

Detection of $\bullet O_2^-$ generation by DHE

The ability of the photosensitizer to produce $\bullet O_2^-$ in aqueous solution was evaluated by choosing DHE as an indicator and crystalline violet (CV) as a standard type I PS reference. A mixture of indicator DHE (30 μM) and **TNPS**, CV or **TNPS**+VC (vitamin C) (10 μM) was exposed to white light and the PL intensity at 600 nm was recorded every 10 s in a PL fluorescence spectrophotometer (excitation wavelength: 510 nm). The intensity of fluorescence enhancement at 600 nm was recorded to indicate the rate of $O_2\bullet^-$ generation.

Cell experiment

Cell culture

HepG2 cells are cultured in DMEM complete medium (supplemented with 10%

fetal bovine serum, 1% penicillin, and streptomycin) at 37 °C in a humidified environment with 5% CO_2. Cells under hypoxia (O_2 concentration of 1 %) was generated with an Anaero Pack® (Mitsubishi Gas Chemical Company, Inc.). The gas-generating bags were placed together with culture medium inoculated with HeLa cells in a sealed hypoxic chamber for 8 hours of hypoxic culture.

Intracellular ROS detection

DCFH-DA was used as an indicator to detect the total ROS production of **TNPS** in cells under light irradiation. At 37°C, HepG2 cells were incubated with **TNPS** aqueous solution in DMEM containing 10% PBS for 1.5 h, and then washed slowly with PBS. Then 10 μM DCFH-DA was added to incubate the cells for 30 min. After the incubation was completed, the culture dish was slowly washed three times with PBS, and then exposed to low-power white light for 5 min, and the fluorescence imaging images of the cells were obtained using a laser confocal microscope. (DCFH-DA, λex = 488 nm, λem = 500-550 nm).

Similarly, DHE was used as an indicator to detect the intracellular $\bullet O_2^-$ production of **TNPS** under light irradiation. HepG2 cells were incubated with **TNPS** aqueous solution in DMEM containing 10% PBS for 1.5 h at 37°C, and then washed slowly with PBS. Then 10 μM DHE was added to incubate the cells for 30 min. After the incubation was completed, the culture dish was slowly washed three times with PBS, and then exposed to low-power white light for 5 min, and the fluorescence imaging images of the cells were obtained using a laser confocal microscope. (DHE, λex = 510 nm, λem = 550-730 nm).

Cell viability test

The MTT assay was used to evaluate the light-induced cytotoxicity of **TNPS** on cancer cells under white light illumination. Aqueous solutions containing different concentrations (0 μM, 5 μM, 10 μM, 15 μM, 20 μM, 25 μM, 30 μM) of **TNPS** were incubated with cells in the dark for 24 h, and then washed slowly with PBS three times, followed by Add 100 uL of freshly prepared MTT solution (0.5 mg/mL) to each sample well, continue to incubate for 3 h, remove the supernatant liquid, and dissolve the precipitate in 100 uL of DMSO. The absorbance of MTT at 570 nm was

measured with a microplate reader (GeniosTecan). As a comparison, the cells were irradiated with low-power white light (70 mW/cm^2) for 10 minutes, then cultured continuously for 12 hours, and then the same concentration of MTT was added to evaluate the cell survival rate under photodynamic conditions.

Live/dead cell staining assay

After co-incubating **TNPS** with HepG2 cells for 1.5 h, they were washed slowly with PBS, and finally irradiated with low-power (70 mW/cm^2) white light for 10 min. Stain with 2 μM calcein-AM and 4 μM propidium iodide (PI) for 30 min, and rinse the residual dye slowly with PBS. The green fluorescence of Calcein-AM and the red fluorescence of PI were observed using a laser confocal microscope, which correspond to live and dead cells, respectively. At the same time, only PBS or **TNPS** or single light is set as the control group. (calcein-AM, λex: 488 nm, λem: 500–540 nm; PI, λex: 568 nm, λem: 600–640 nm).

Apoptosis detection

HepG2 cells were seeded in 6-well plates at a density of 1 × 10^4 cells per well and allowed to adhere for 24 hours. They were randomly divided into four groups: PBS, PBS + Laser, **TNIS-TEG**, and **TNIS-TEG** + Laser. The cells were incubated with PBS or **TNIS-PEG** (50 × 10^{-6} M) in the dark for 1.5 hour. In the laser groups, after irradiation with low-power white light for 10 minutes, the cells were incubated for an additional 2 hours. The supernatant was removed, and the cells were washed three times with PBS before being digested with trypsin to obtain a cell suspension, which was then washed twice with pre-cooled PBS. Finally, the cells were incubated on ice with dye from the apoptosis kit for 15 minutes prior to measurement. Cell apoptosis was detected using multicolor flow cytometry analysis.

Animal experiment

Animal tumor models

Eight-week-old female BALB/c-nu nude mice were purchased from Chongqing Tengxin Huafu Laboratory Animal Sales Co, Ltd, and housed in a specific pathogen-free (SPF) environment.After one week of adaptation, each nude mouse was subcutaneously injected with 100 μL of HepG2 cell suspension (1×10^6 cells) in the

right hind limb to establish the tumor model. The tumor growth was dynamically monitored thereafter. All animal experiments were conducted following the guidelines of the Animal Experiment Ethics Committee of Southwest Medical University.

In Vivo Tumor PDT Capability

The constructed HepG2 tumor-bearing nude mouse model was divided into four groups: Group G1: PBS, Group G2: PBS + laser, Group G3: **TNIS-TEG**, and Group G4: **TNIS-TEG** + laser. Groups G1 and G2 received intra-tumoral injection of 100 μL PBS, while Groups G3 and G4 received intra-tumoral injection of 100 μL **TNIS-TEG** (200 μM).

Thirty minutes post-injection, Groups G2 and G4 were exposed to continuous light from a white LED lamp at a power density of 200 mW/cm² for 10 minutes. After one photodynamic therapy (PDT) session, body weight and tumor volume of each nude mouse were monitored bi-daily.

On the 14th day, blood samples were obtained via orbital bleeding method to collect whole blood and serum for hematological and biochemical analysis. Subsequently, the mice were euthanized by cervical dislocation, tumors and major organs (heart, liver, spleen, lung, kidney) were then excised, weighed, and fixed in 4% paraformaldehyde solution for subsequent H&E staining.

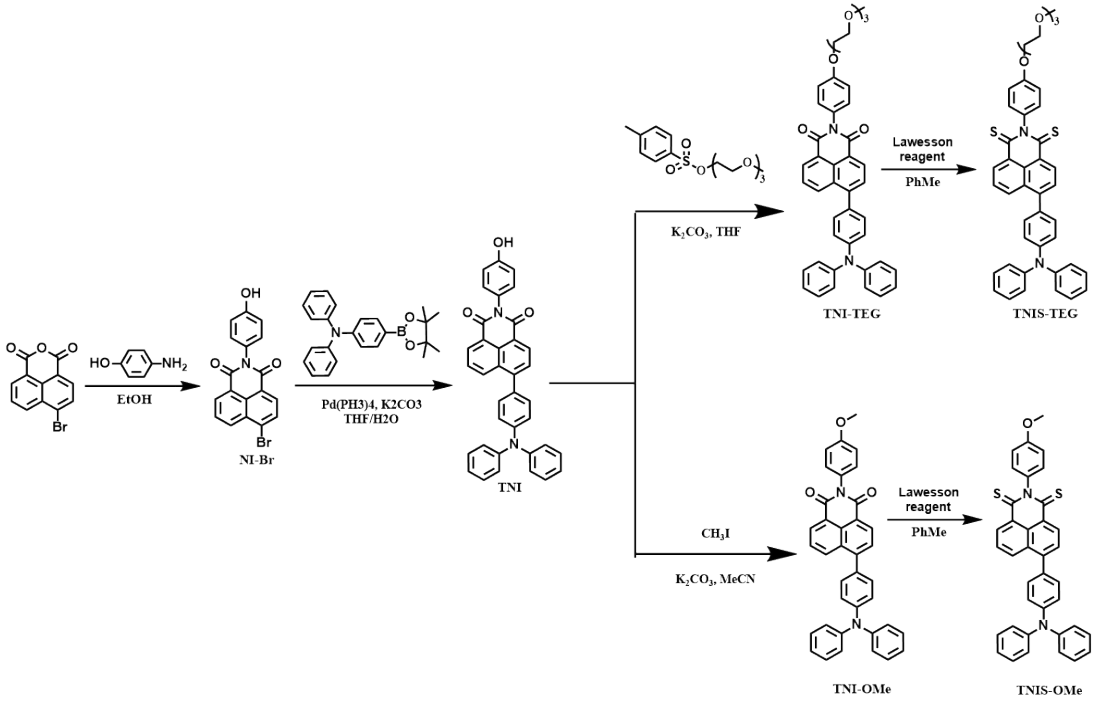

Scheme S1 The synthesis route of target compounds

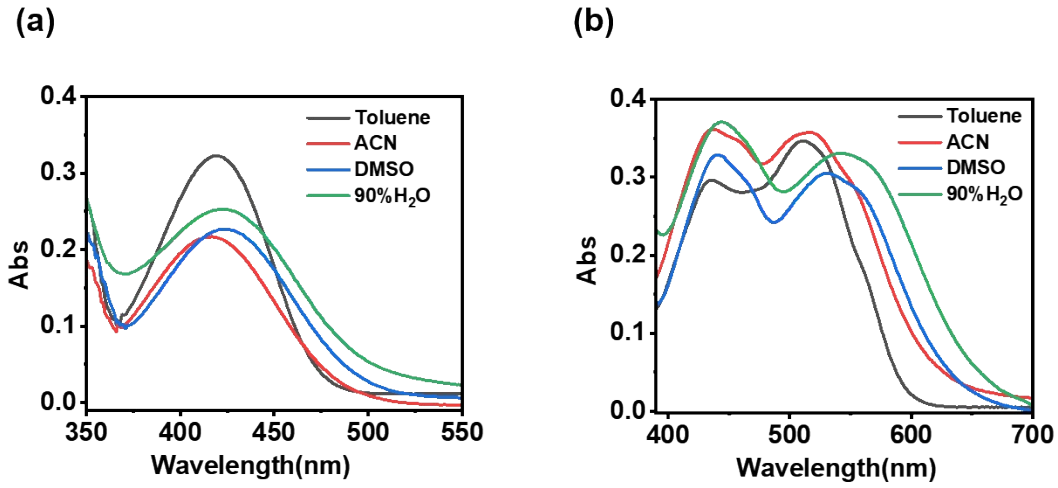

Fig. S1 Absorption spectra of (a) **TNI-OMe** and (b) **TNIS-OMe** in different solvents.

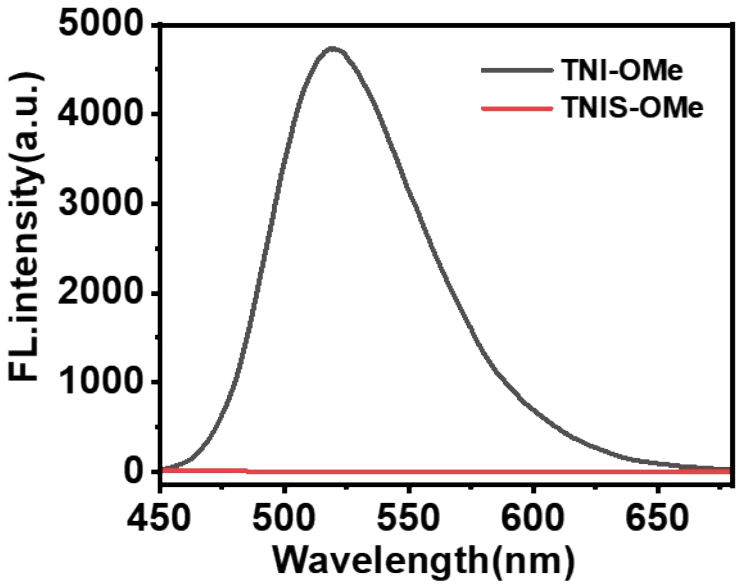

Fig. S2 Fluorescence emission spectra of **TNI-OMe** and **TNIS-OMe** in ACN solution (c = 10 μM, λex = 405 nm)

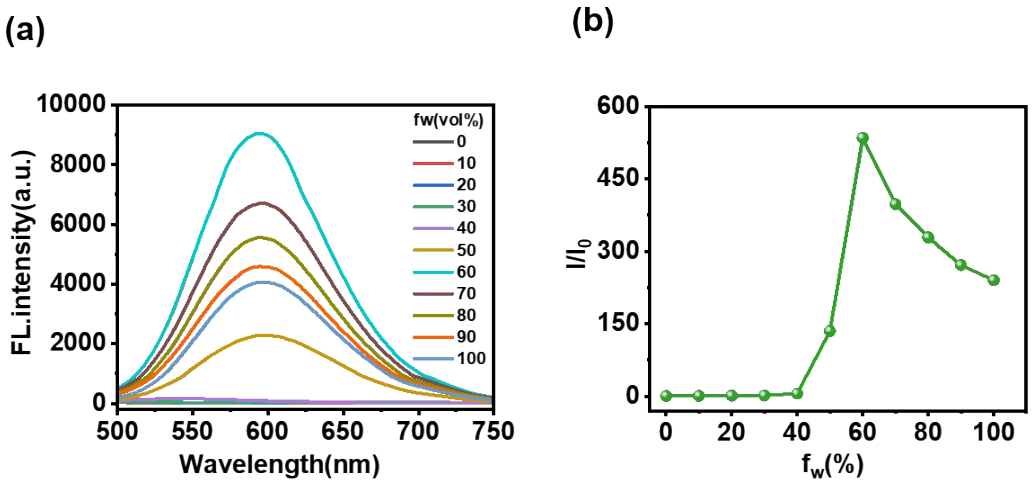

Fig. S3 PL spectra (a) and the relative fluorescence emission intensity at 580 nm of **TNI-TEG** (10μM) in different water fractions (fw%) of DMSO/water mixtures. (b) Relative fluorescence emission intensity of **TNI-TEG** at 580 nm with different water fractions.

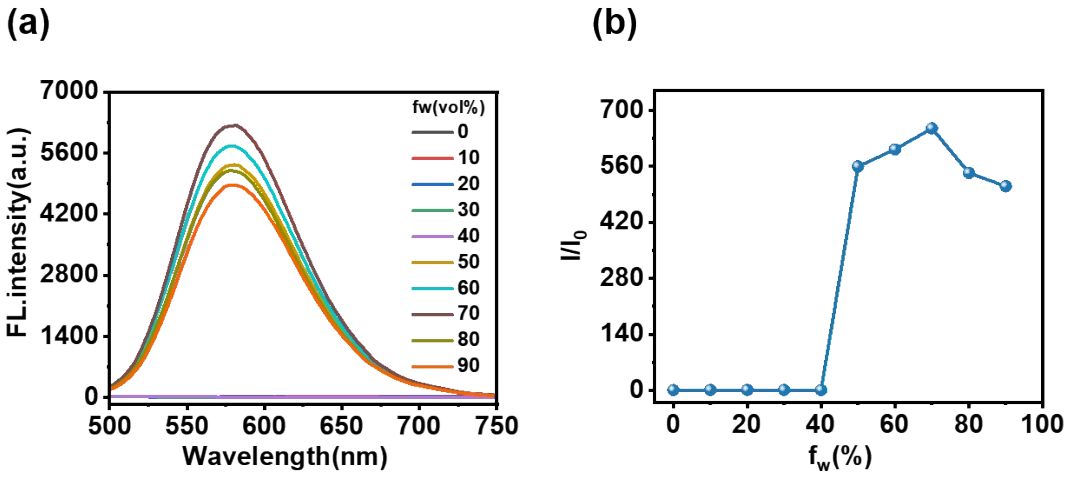

Fig. S4 PL spectra (a) and the relative fluorescence emission intensity at 580 nm of **TNI-OMe** (10 μM) in different water fractions (fw%) of DMSO/water mixtures. (b) Relative fluorescence emission intensity of **TNI-TEG** at 580 nm with different water fractions.

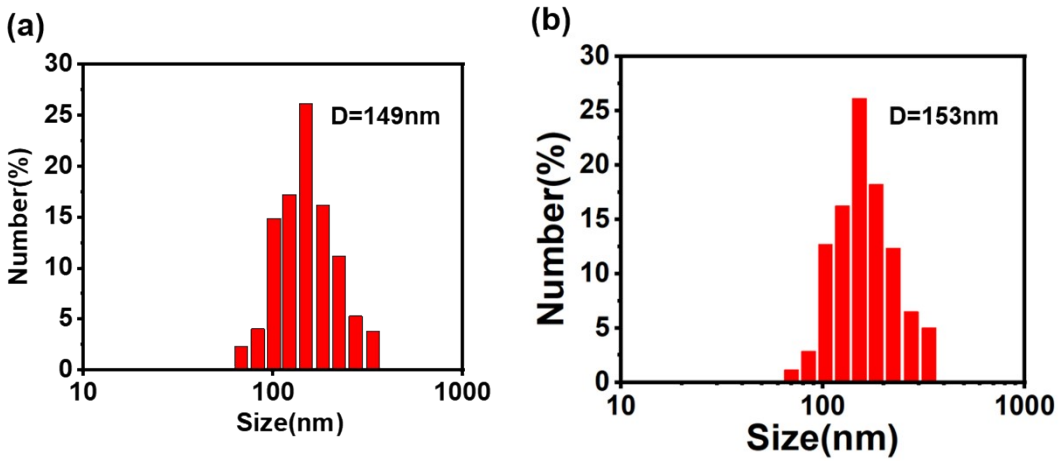

Fig. S5 Average size change of **TNIS-TEG** NPs after (a) 7days and (b) 14 days of storage in deionised water at room temperature analysed by DLS.

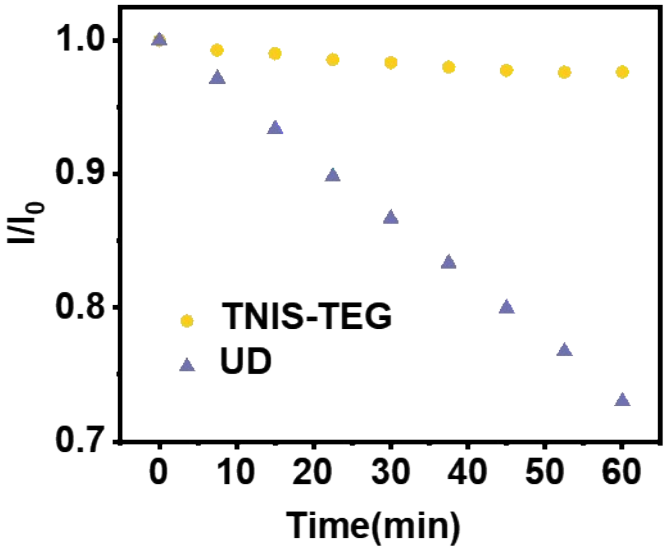

Fig. S6 Photostability of **TNIS-TEG**.

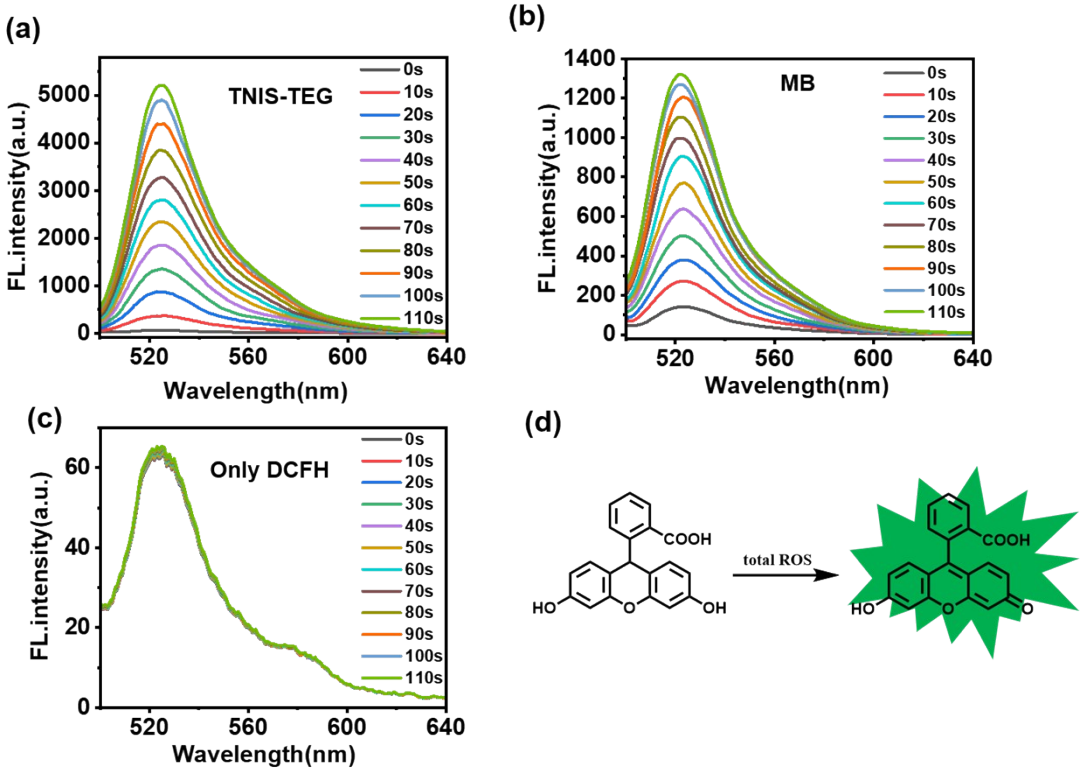

Fig. S7 Time-dependent fluorescence spectra changes of DCFH (10 μM) and (a) **TNIS-TEG** (10 μM), (b) MB (10 μM), (c) blank in water after irradiation for different time; (d) Schematic diagram of the action of the total ROS fluorescent indicator DCFH. EX: 490 nm.

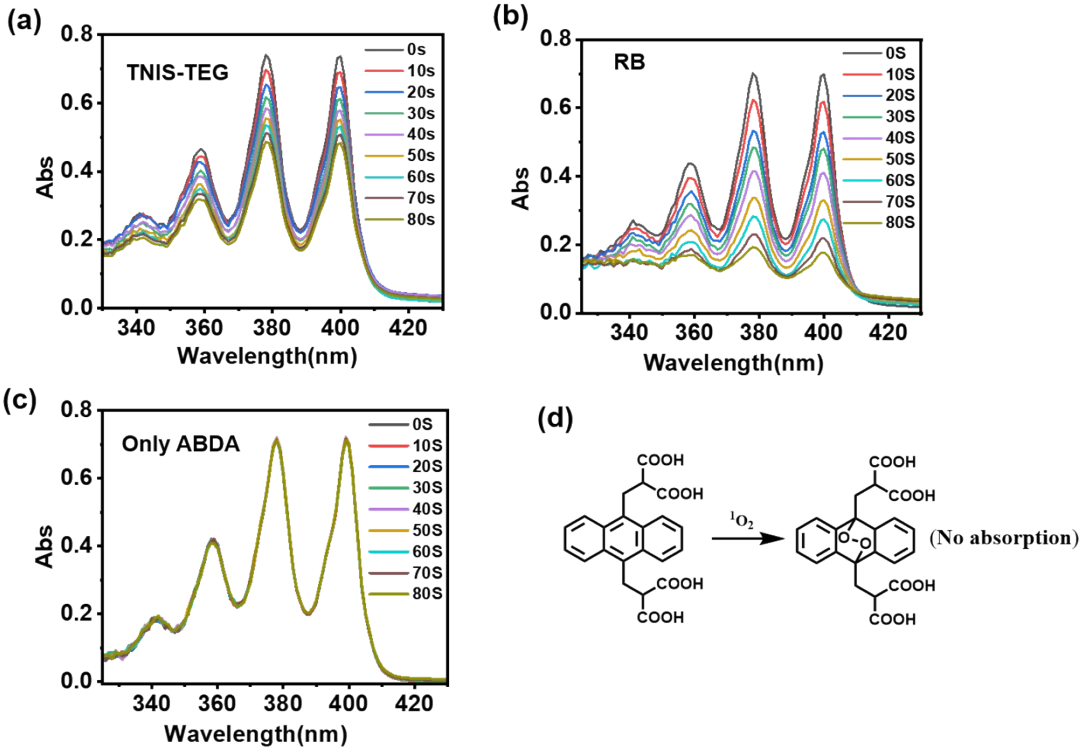

Fig. S8 Time-dependent absorption spectra changes of ABDA(60 uM)in the presence of (a)

TNIS-TEG (10 uM), (b) Rose Bengal (10 uM), (c) blank in water after irradiation for different time; (d) Schematic diagram of the action of singlet oxygen indicator ABDA.

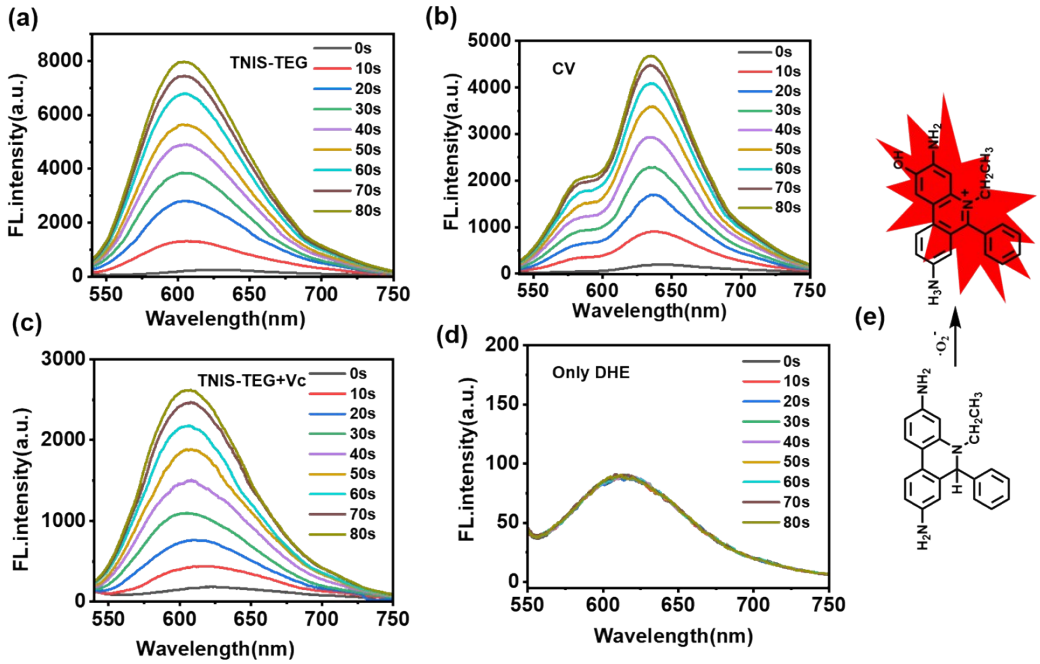

Fig. S9 Time-dependent fluorescence spectra changes of mixtures of DHE (30 μM) and (a) **TNIS-TEG** (10 μM), (b) CV (10 μM), (c) **TNIS-TEG**+VC (30 μM), (d) blank in water after irradiation for different time; (e) Schematic diagram of the action of superoxide radical fluorescent indicator DHE.

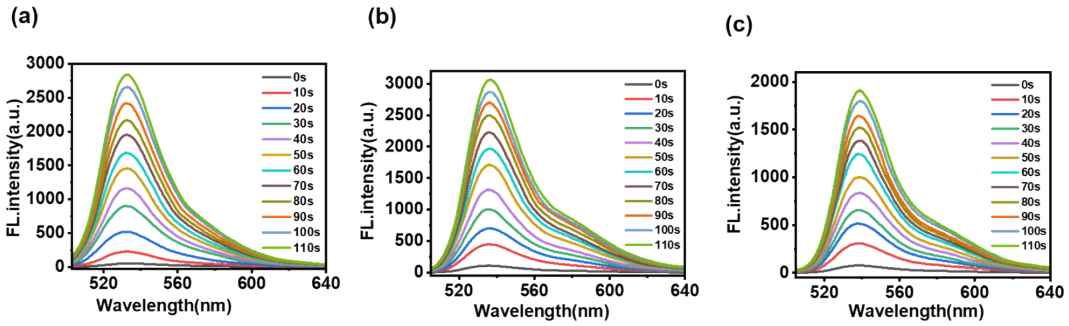

Fig. S10 In the presence of **TNIS-TEG**, time-dependent fluorescence spectra changes of DCFH in (a) THF, (b) ACN, (c) DMSO after different exposure times.

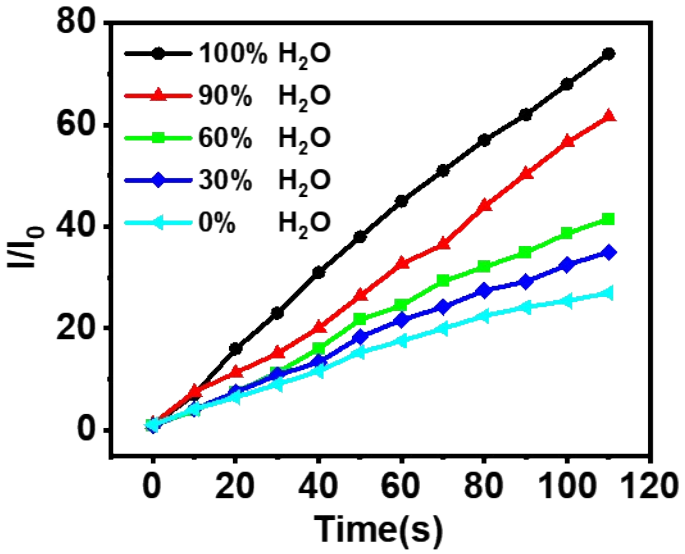

Fig. S11 Relative emission intensity of DCFH at 525nm in different fraction of H_2O-CH_3CN mixture in the presence of **TNIS-TEG**.

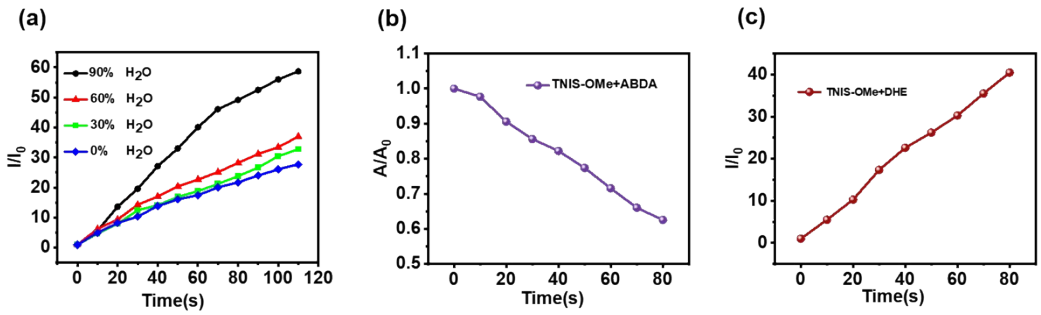

Fig. S12 (a) Relative emission intensity of DCFH at 525nm in different fraction OF H_2O-CH_3CN mixture in the presence of **TNIS-OMe**; (b) Relative absorbance of ABDA at 378 nm in the presence of **TNIS-TEG**; (c) Relative emission intensity of DHE at 615 nm in the presence of **TNIS-OMe**.

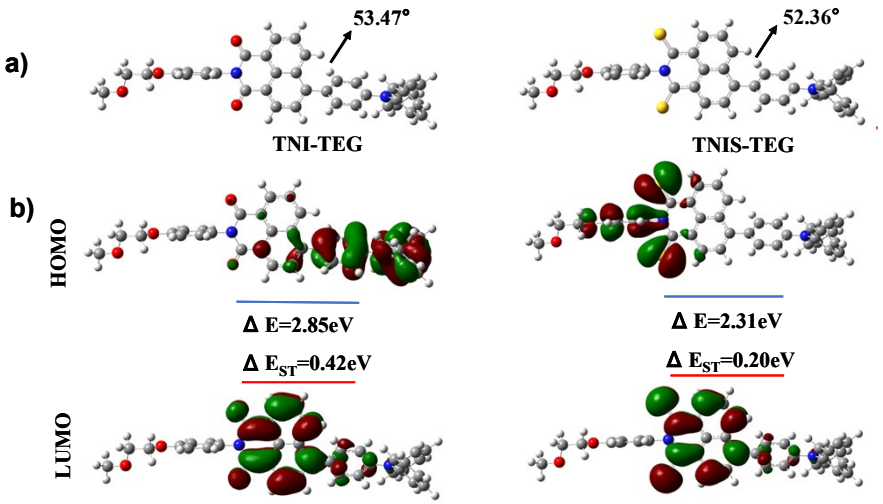

Fig. S13 a) Optimum geometries of **TNI-TEG** and **TNIS-TEG**. b) The distribution of the HOMO and LUMO orbitals and the energy gap between the S_1 and T_1 states of **TNI-TEG** and **TNIS-TEG** by TD-DFT calculations based on the B3LYP/6-31G basis set.

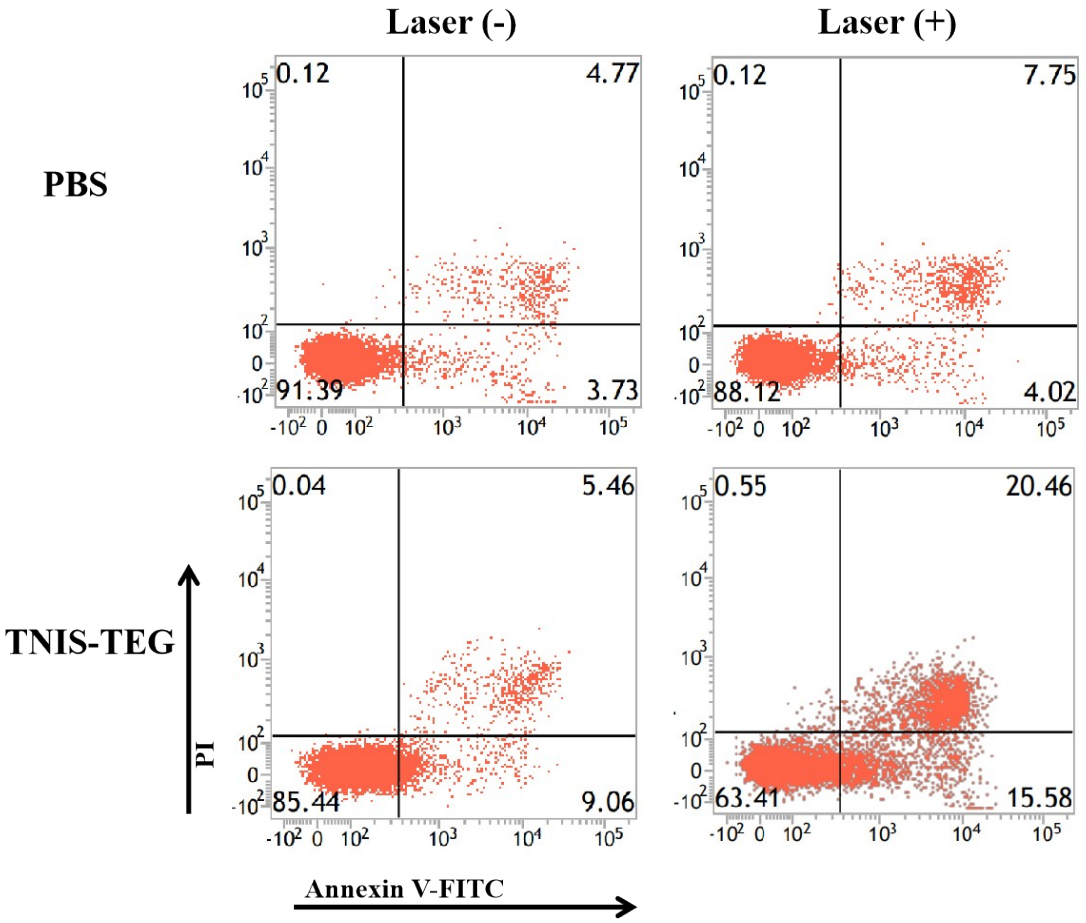

Fig. S14 Flow cytometry results for **TNIS-TEG** (50 μM) induced HepG2 cell apoptosis after different treatments.

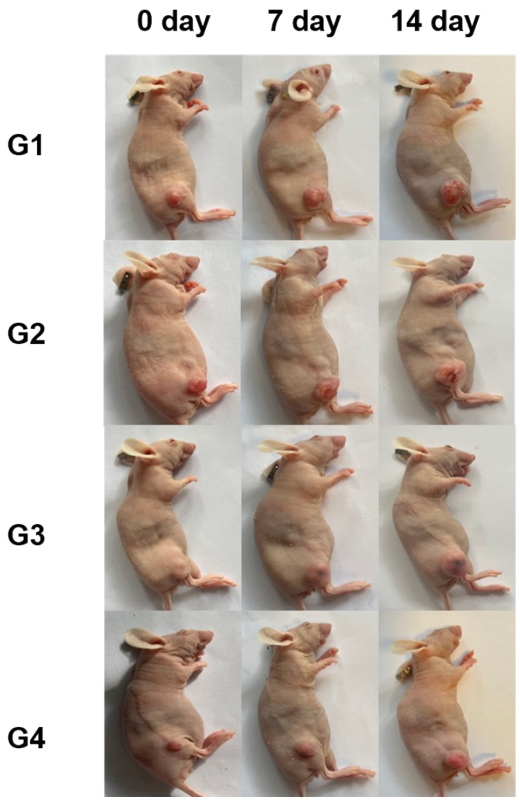

Fig. S15 Photographs of mice in the four groups before and after therapy

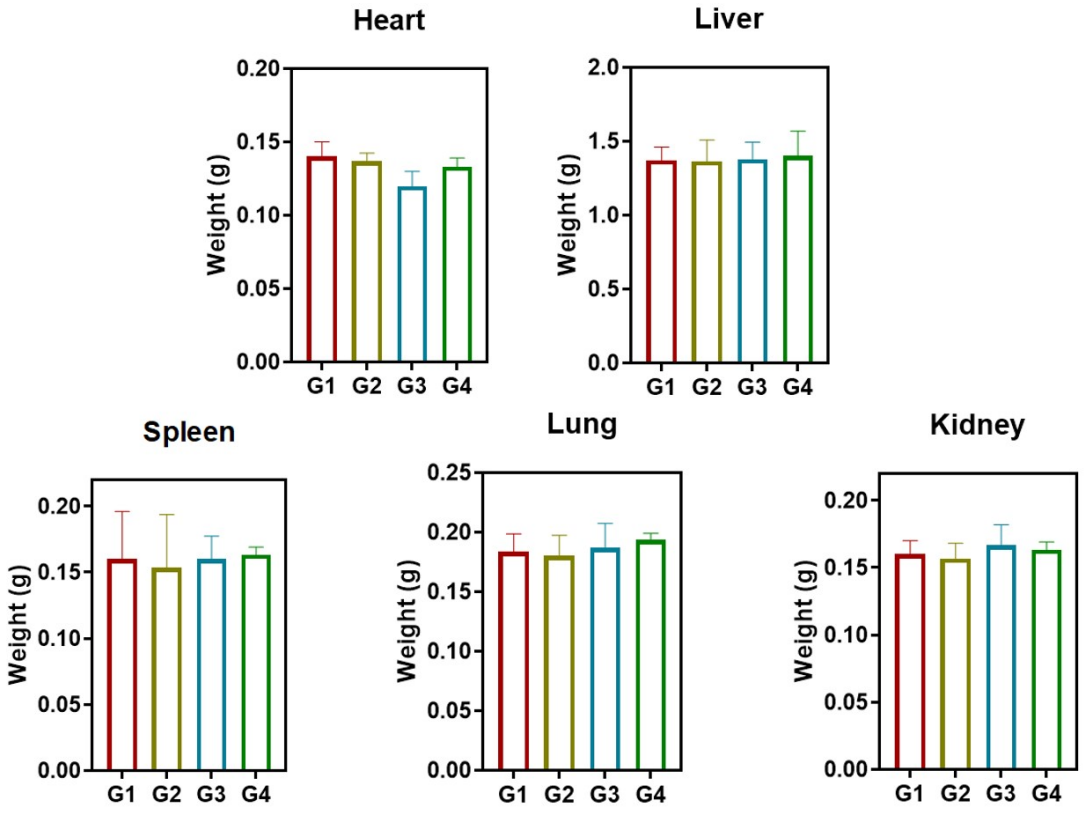

Fig. S16 Weights of major organs in different groups after 14 days of treatment.

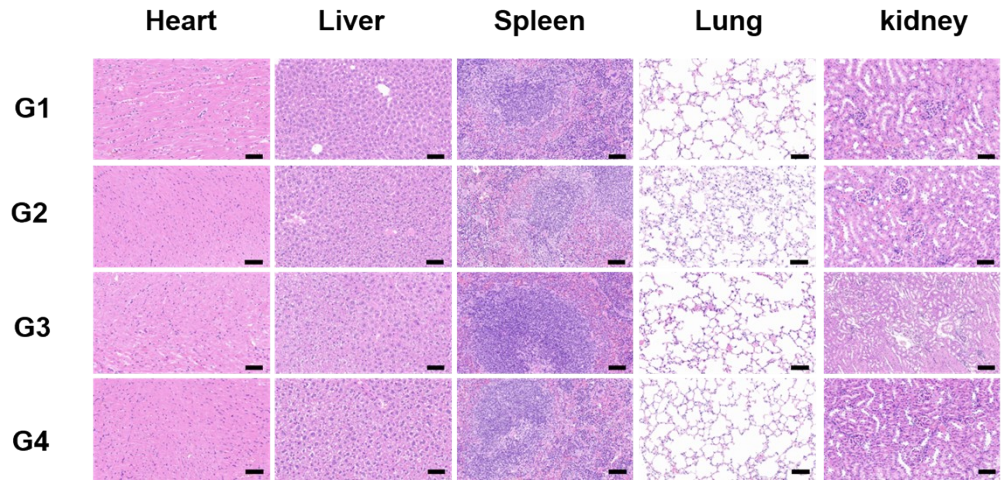

Fig. S17 H&E staining of the major organs of the mice in different groups after 14 days of treatment (scale: 100 μm).

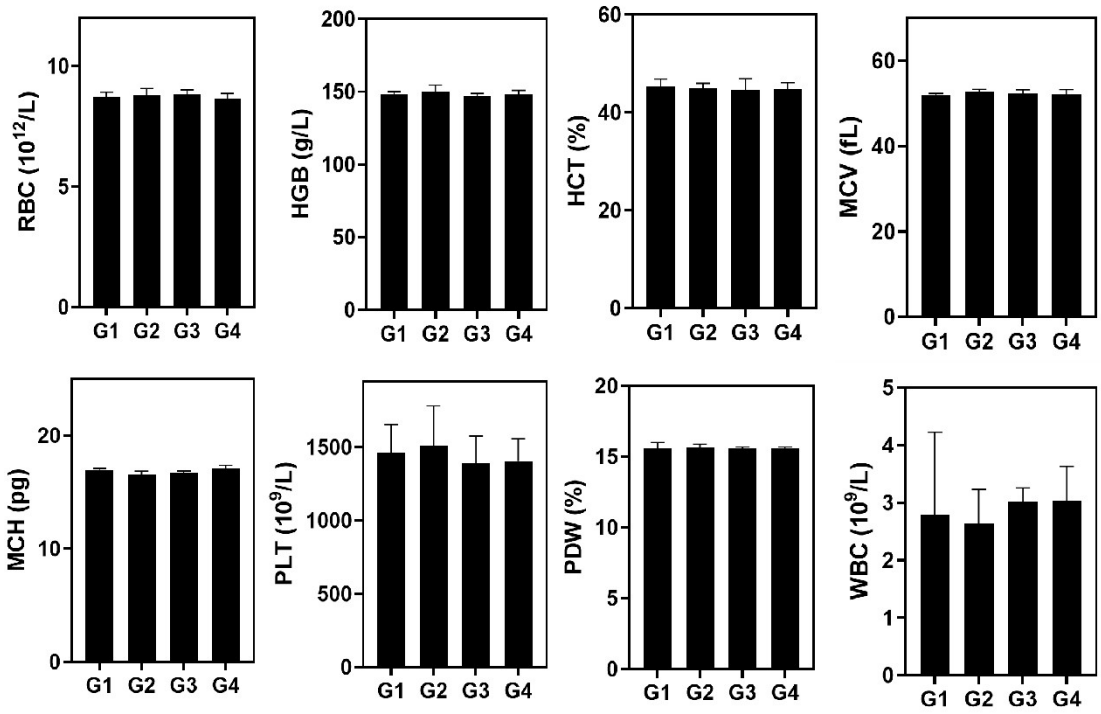

Fig. S18 Blood cell indicators in mice from different groups after 14 days of treatment.

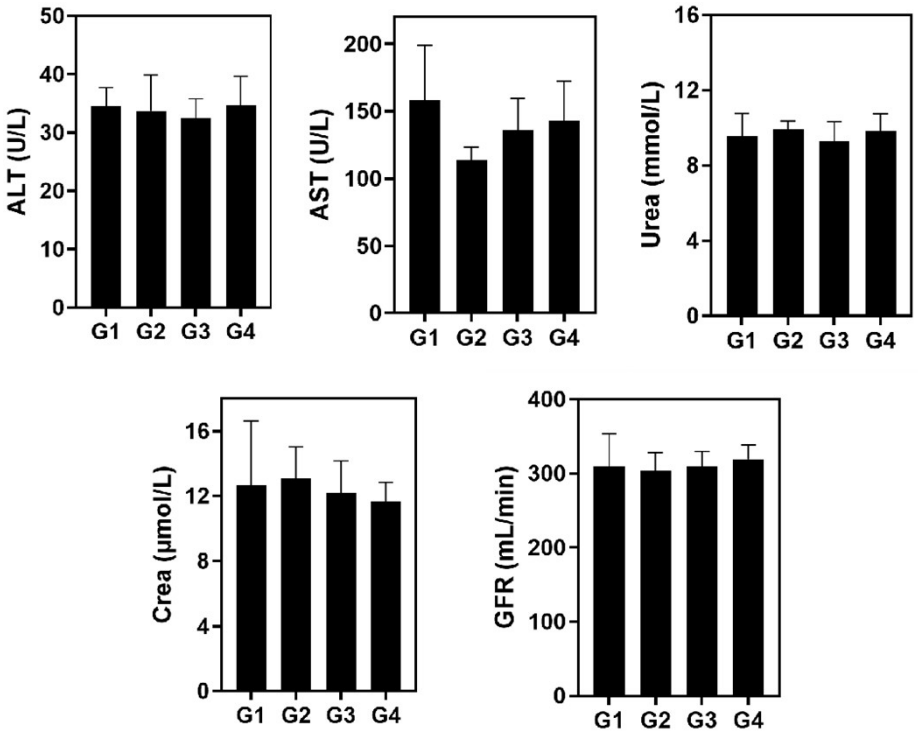

Fig. S19 Blood biochemistry parameters in mice from different groups after 14 days of treatment.

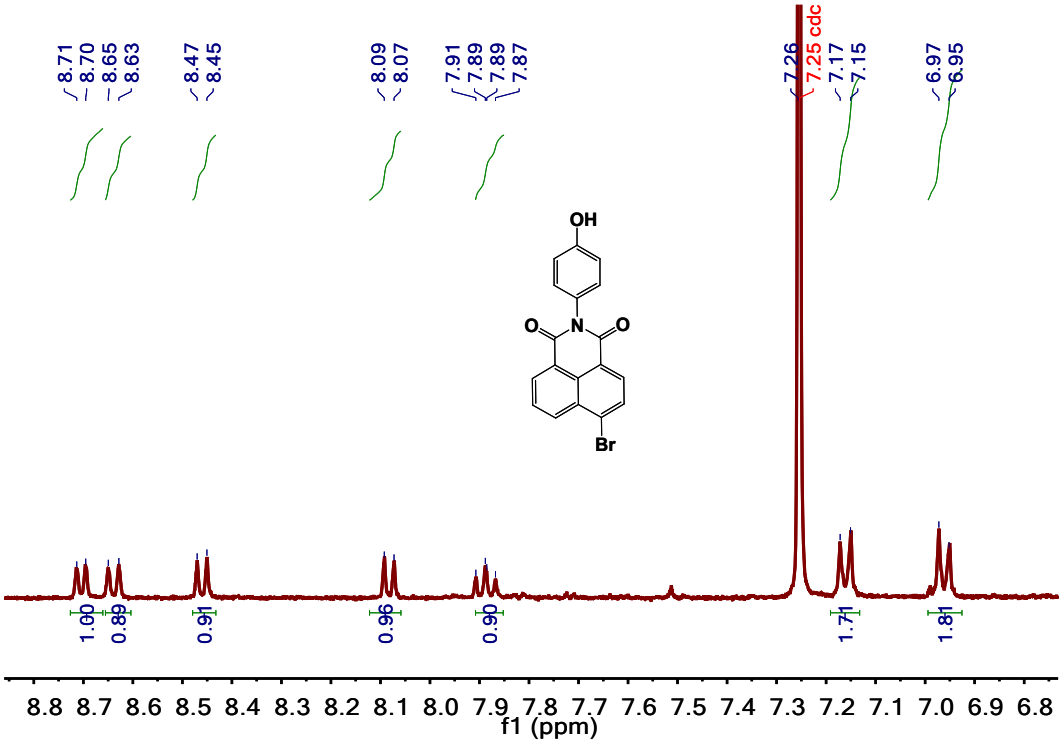

Fig. S20 ^{1}H NMR spectrum of NI-Br in $CDCl_3$ solution

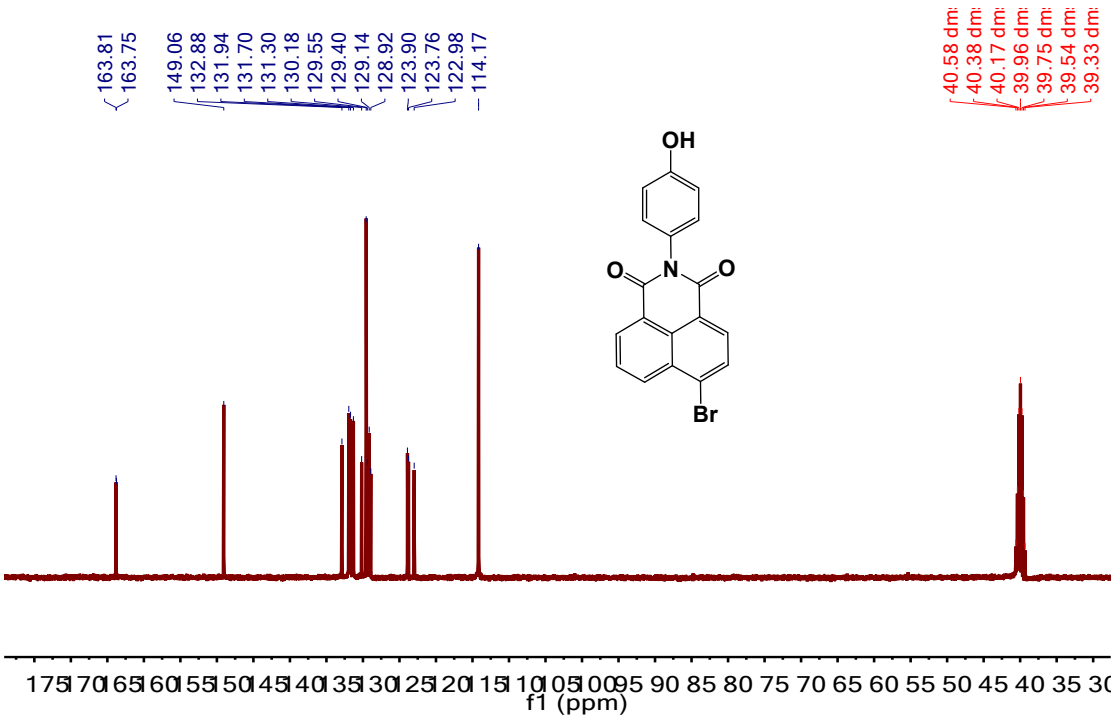

Fig. S21 ^{13}C NMR spectrum of NI-Br in $CDCl_3$ solution

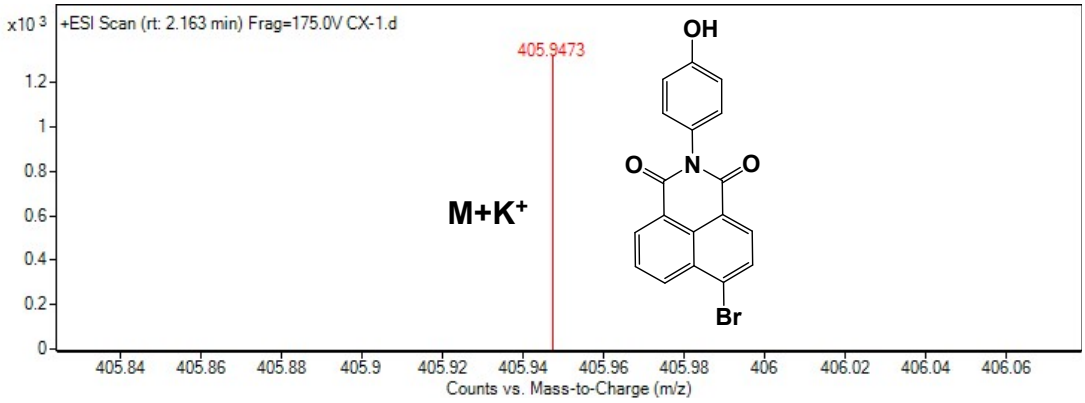

Fig. S22 HRMS spectrum of NI-Br

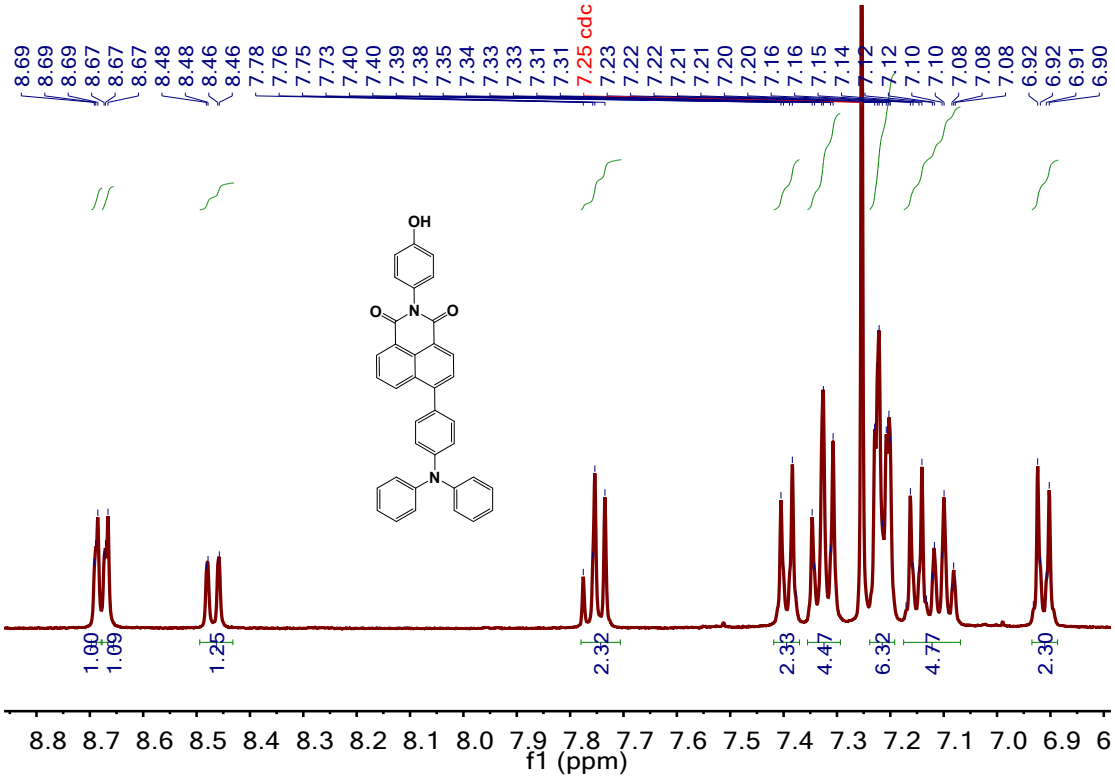

Fig. S23 ^{1}H NMR spectrum of **TNI** in $CDCl_3$ solution

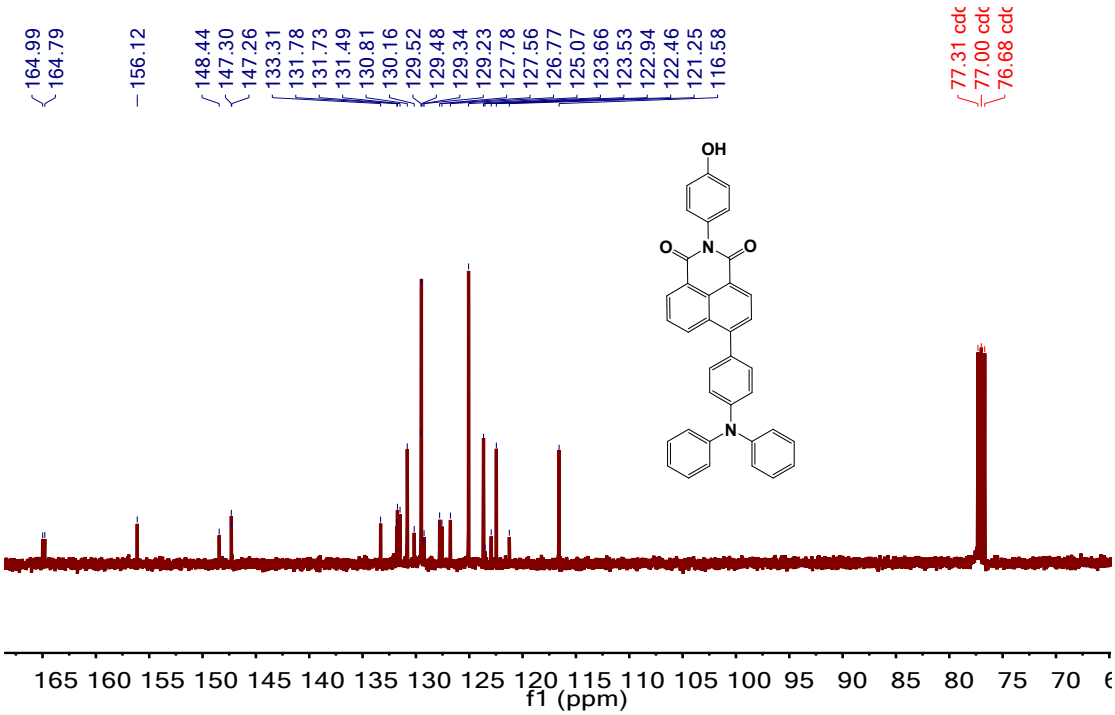

Fig. S24 ^{13}C NMR spectrum of **TNI** in $CDCl_3$ solution

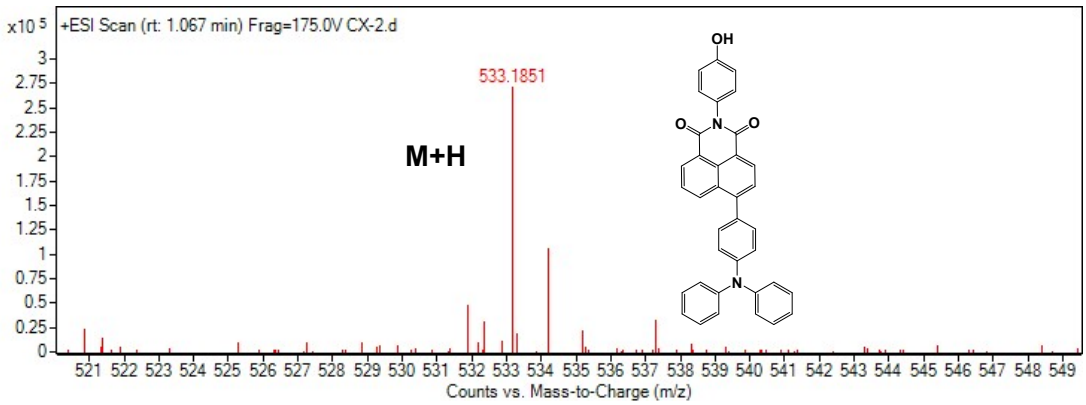

Fig. S25 HRMS spectrum of **TNI**

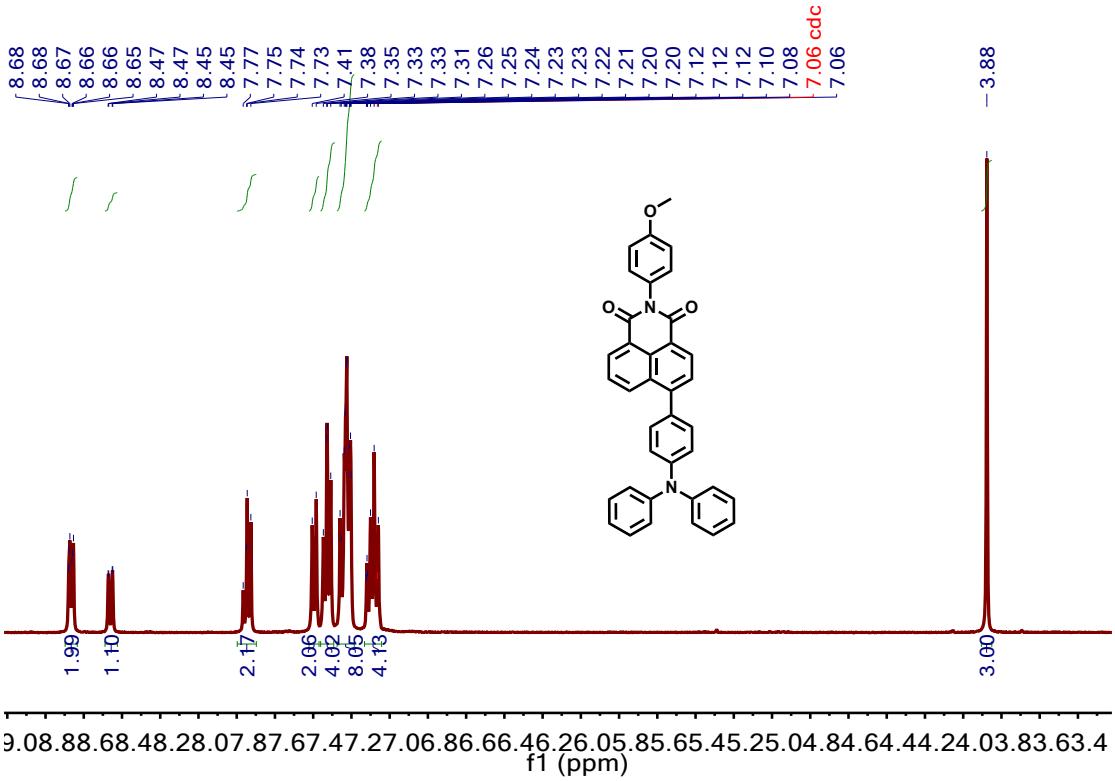

Fig. S26 ^{1}H NMR spectrum of **TNI-OMe** in $CDCl_3$ solution

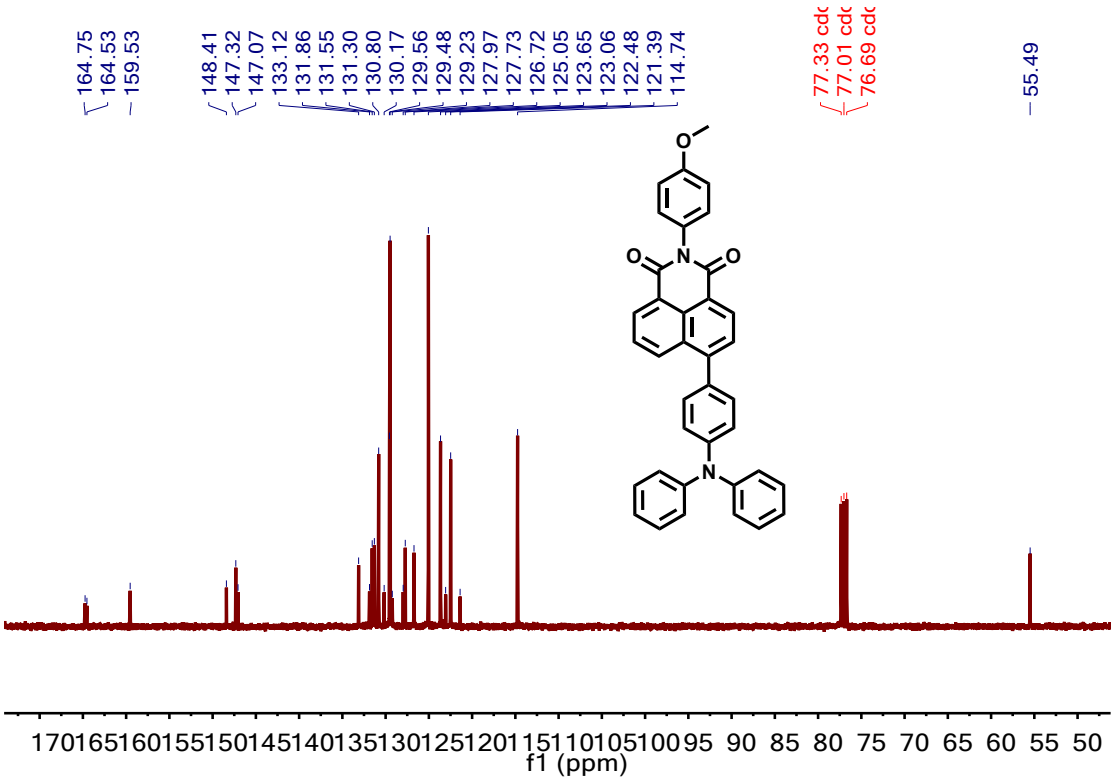

Fig. S27 ^{13}C NMR spectrum of **TNI-OMe** in $CDCl_3$ solution

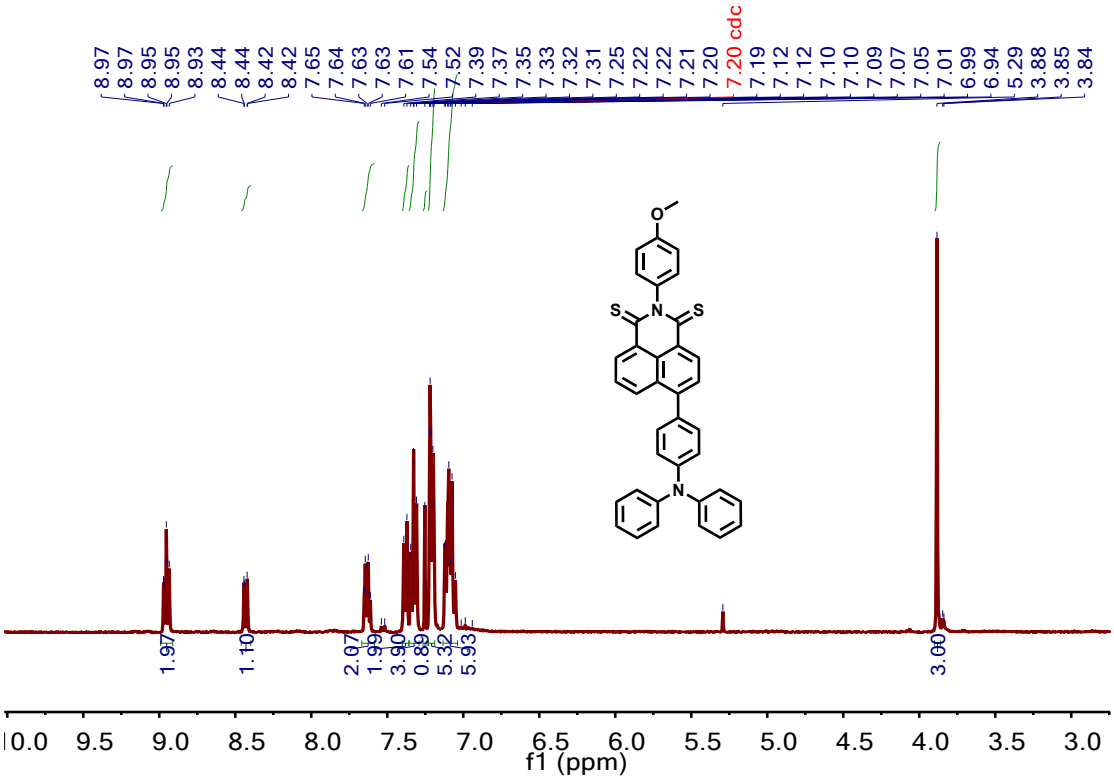

Fig. S28 ^{1}H NMR spectrum of **TNIS-OMe** in $CDCl_3$ solution

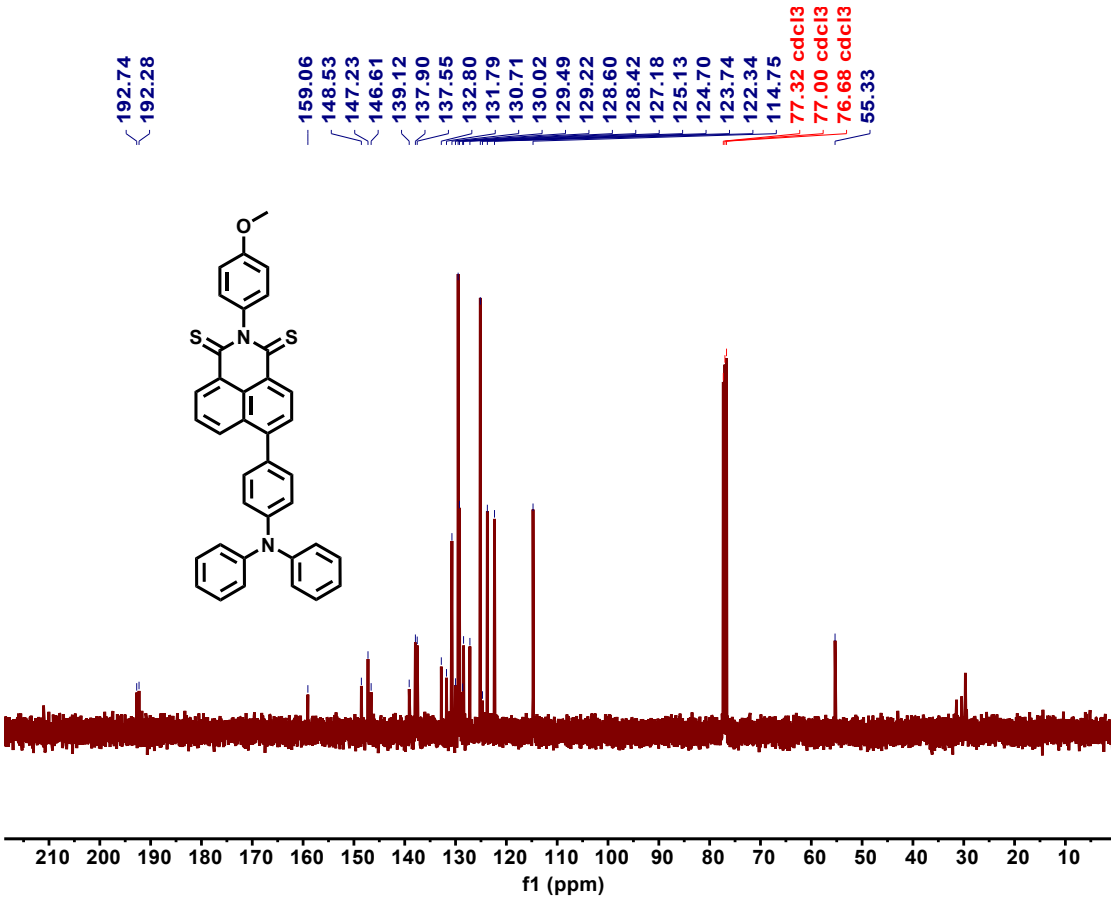

Fig. S29 ^{13}C NMR spectrum of **TNIS-OMe** in $CDCl_3$ solution

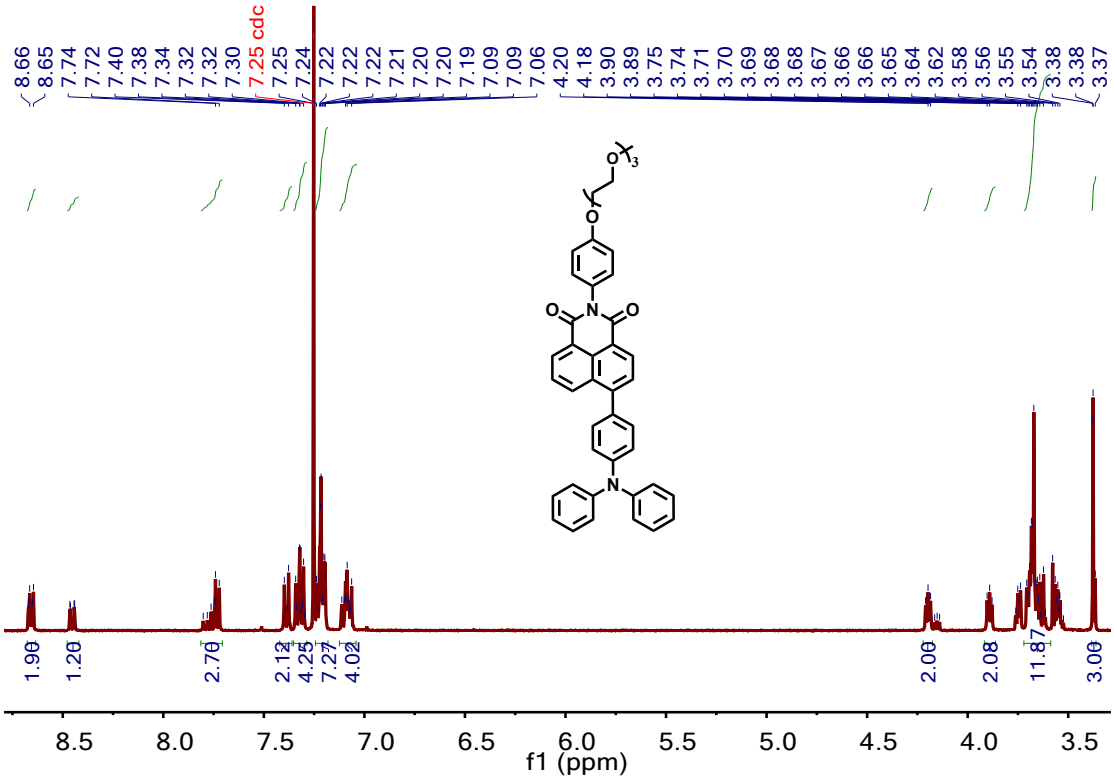

Fig. S30 ^{1}H NMR spectrum of **TNI-TEG** in $CDCl_3$ solution

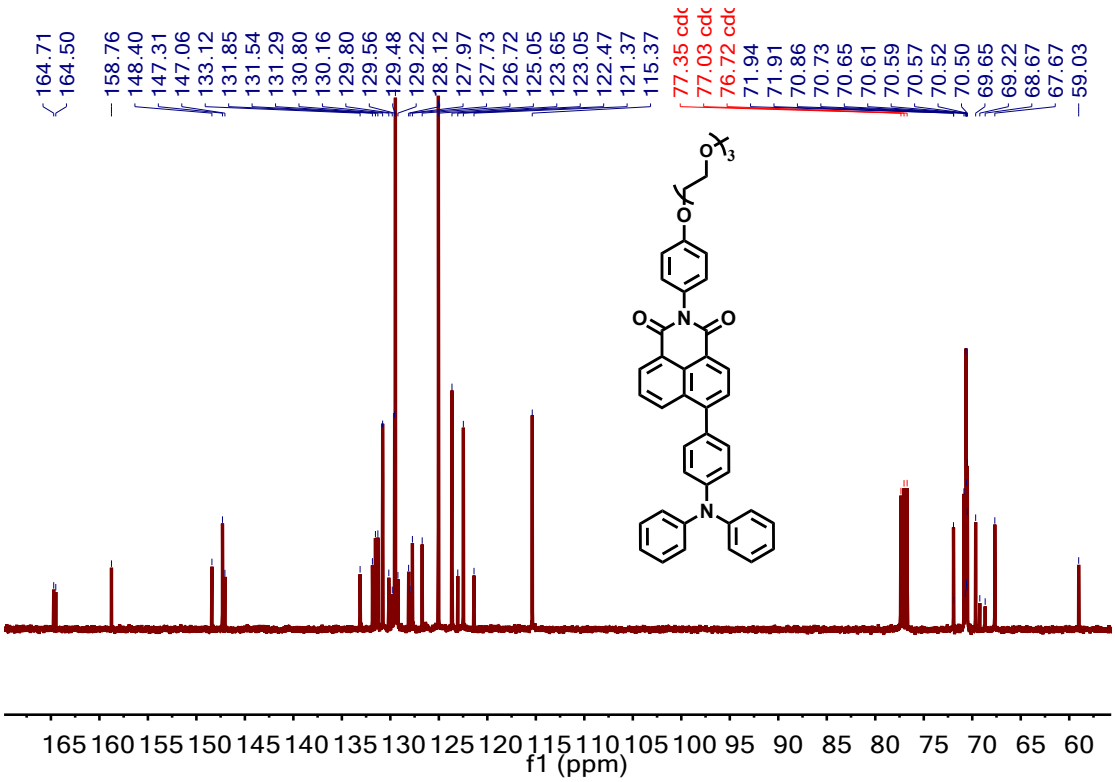

Fig. S31 ^{13}C NMR spectrum of **TNI-TEG** in $CDCl_3$ solution

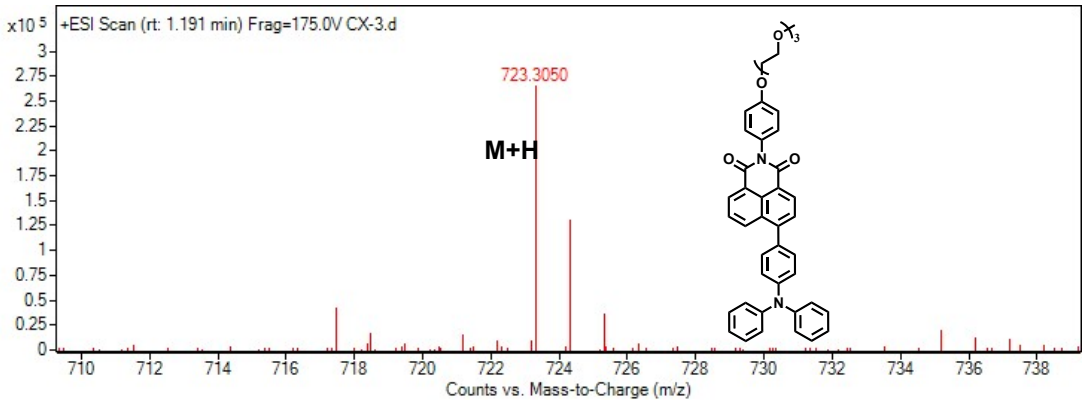

Fig. S32 HRMS spectrum of **TNI-TEG**

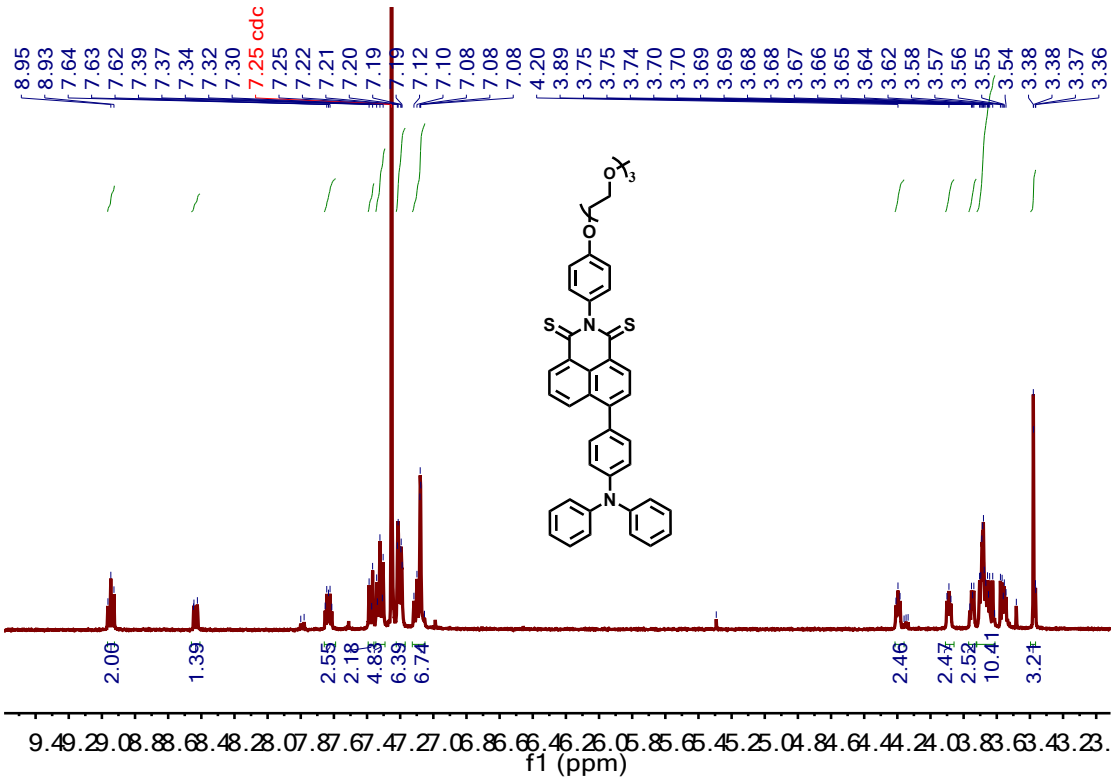

Fig. S33 ^{1}H NMR spectrum of **TNIS-TEG** in $CDCl_3$ solution

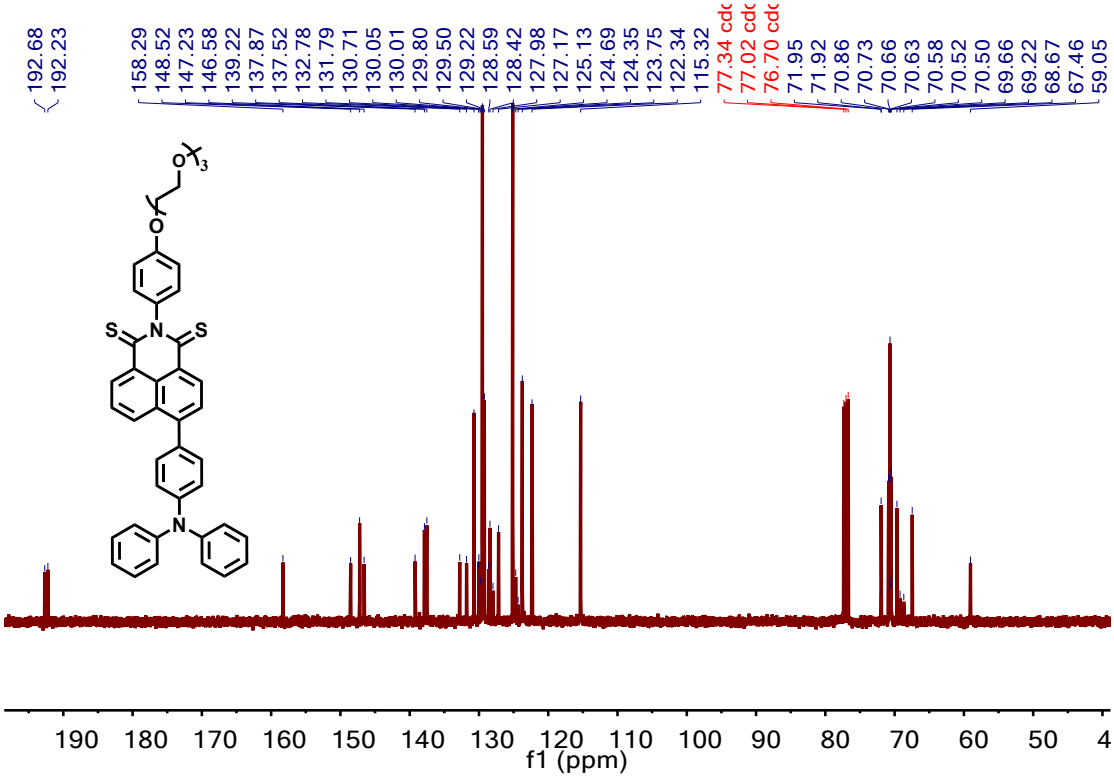

Fig. S34 ^{13}C NMR spectrum of **TNIS-TEG** in $CDCl_3$ solution

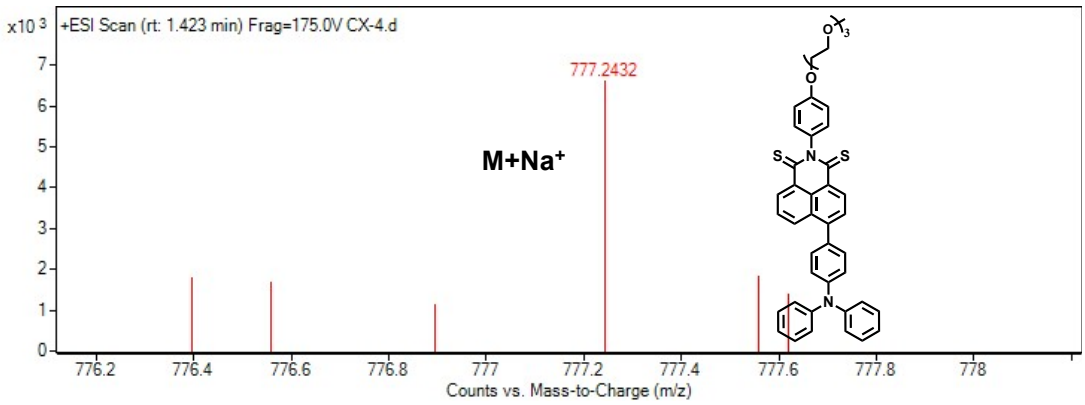

Fig. S35 HRMS spectrum of **TNIS-TEG**